

Single-Event Upsets in 3D Gaussian Splatting Rendering: Bit-Level Criticality, Spatial Extent, and a Parallel Support Guard

Faruk Alpay* Barış Başaran

Department of Computer Engineering, Bahçeşehir University, Istanbul, Turkey
{faruk.alpay, baris.basaran}@bahcesehir.edu.tr

Abstract

Three-dimensional Gaussian splatting is a standard real-time scene representation, and it is increasingly deployed on hardware that is exposed to transient faults: spaceborne and avionic processors, mobile and robotic edge devices, and rendering clusters in which silent data corruption is a documented operational reality. A trained model is a large array of floating-point parameters resident in GPU memory, so a single-event upset corresponds to a single flipped bit in one of those values. This paper measures the effect of such upsets on the rendered image and uses the result to construct a defense. A GPU-resident parallel fault-injection engine applies more than 3.8 million controlled single-bit upsets across four trained scenes, six parameter fields, all bit positions, and three numeric formats (`fp32`, `fp16`, `bf16`), using 5.3 GPU-hours of GPU time. The effect is concentrated. Most single-bit upsets leave the image perceptually unchanged because the representation is highly redundant, while a small set of high-order bits, principally the sign bit of the logarithmic scale, enlarge a single primitive until it covers up to 75.7% of the frame. A closed-form perturbation bound derived from the IEEE-754 layout and the activation functions of the splatting pipeline predicts the per-bit ordering and is validated against the measurements. The concentration motivates a support guard: a per-primitive clamp of each parameter to the coordinate box observed during training, at a cost of 76 μ s per frame. Over 768,000 guarded upsets the worst observed corruption footprint is 11.68% of the frame; we prove that the guard leaves a clean model unchanged and that no single-bit upset can produce frame-covering corruption under it. Under accumulated dose the unguarded renderer degrades to 10.6 dB at 20,000 simultaneous upsets, whereas the guarded renderer remains at 21.8 dB. The corruption footprint also gives the number of screen tiles, and therefore compositing nodes, that a single upset contaminates in a distributed renderer, where the per-node guard contains it.

1 Introduction

Real-time radiance-field rendering with 3D Gaussian splatting (3DGS) [9] has moved quickly from a novel-view-synthesis result to an infrastructure component. It underlies simultaneous localization and mapping on robots [13], it is being pushed onto mobile and embedded accelerators, and it is rendered at scale in data centers. These deployments share a property that is rarely considered in real-time rendering: the hardware is not perfectly reliable. Cosmic-ray and alpha-particle strikes flip bits in memory and registers [17, 1], and the rate is high enough that fleet operators now report

*Correspondence: alpay@lightcap.ai

silent data corruption as a routine cause of wrong results [2, 6]. Graphics processors, the substrate on which 3DGS runs, have been shown under accelerated neutron beams to be particularly exposed [18, 3].

A trained 3DGS model is a large array of floating-point numbers held in GPU memory: for each primitive, a position, an anisotropic scale, an orientation quaternion, an opacity, and a set of spherical-harmonic color coefficients. A single-event upset (SEU) in that memory is, to first order, a single flipped bit in one of those numbers. The corresponding question for deep network weights has been studied extensively, and there a small number of well-chosen bit flips can destroy a classifier [19, 11, 10]. The 3DGS case differs structurally: a network weight is shared across an entire output, whereas a Gaussian primitive contributes to a small spatial region of one image, and a scene contains hundreds of thousands of primitives. Whether this redundancy makes the representation robust, or instead concentrates the risk into a few rare failures, has not been established. This paper resolves it by direct measurement and then derives a defense from the measured structure.

Estimating a per-bit, per-field catastrophe rate requires thousands of independent samples per cell, and there are hundreds of cells per scene and precision. The fault-injection engine is therefore designed for throughput rather than latency: it renders a stream of independently corrupted models at hundreds of corrupted renders per second, and the campaign produces more than 3.8 million measured upsets. The same campaign on a single-threaded CPU rasterizer is estimated at roughly 178 CPU-days; on the GPU it used 5.3 GPU-hours.

The contributions are as follows.

- **Bit-level criticality.** Single-bit SEU risk in 3DGS is highly concentrated. The median upset is perceptually invisible, and the dominant case is the sign bit of the logarithmic scale: flipping it enlarges a single primitive to cover a mean of 10.3% and up to 75.7% of the image (Section 5.1).
- **A predictive perturbation bound.** A closed-form bound from the IEEE-754 layout [8] and the splatting activations predicts the per-bit severity ordering, including why the scale and opacity activations make their sign and high exponent bits the dominant ones; it is validated against the data (Section 4, Section 5.2).
- **A support guard.** The catastrophic upsets are exactly those that push a value outside the trained parameter range. A per-primitive clamp to the per-field support box neutralizes 90.4% of them at a cost of 76 μ s per frame, leaves a clean model unchanged, and is proved to make frame-covering corruption impossible under any single-bit upset (Theorem 1, Theorem 2, Section 5.5).
- **Accumulated dose and distributed rendering.** The unguarded representation absorbs many simultaneous upsets through redundancy but eventually degrades; with the guard the rendered quality stays close to clean across the tested dose range, up to 20,000 simultaneous upsets (Section 5.4). In a distributed renderer the spatial extent of a corrupted primitive equals the number of screen tiles, and therefore compositing nodes, that a single upset contaminates, and the node-local guard contains it at the source (Section 5.10).
- **Scaling, design space, reliability, and prediction.** Resilience to accumulated corruption grows with primitive count while per-upset severity does not (Section 5.6); the support guard matches error-correcting and duplication schemes at a fraction of their cost (Section 5.8); under representative orbital upset rates the estimated mean time between catastrophic frames moves from days to beyond mission duration once the guard is applied (Section 5.9); and a classifier predicts catastrophic bits from the field and bit position alone at an area under

the ROC curve of 0.997, so future models can be screened without an injection campaign (Section 5.11).

We release the fault-injection engine, the full analysis, the aggregated per-cell records, and the logs, with training and campaign code that regenerates the models and the raw per-injection records exactly, so that the campaign can be reproduced and extended.¹

2 Background and Related Work

Soft errors and silent data corruption. A single-event upset is a transient change of stored state caused by ionizing radiation [17, 1, 16]. At terrestrial scale the dominant source is the atmospheric neutron flux; in space and avionics the flux is higher and the consequences are safety relevant. Two industrial studies brought the topic into mainstream computing by showing that production fleets experience silent, undetected wrong results at rates far above what classical soft-error models predict, and that the corruptions are data and core dependent [2, 6]. Graphics processors specifically have been characterized under accelerated neutron beams, where both the error rate and the fraction of errors that survive to the output depend strongly on the workload and the data type [18, 3]. Our work is downstream of these: we take the existence of bit flips as given and ask what a 3DGS renderer does with one.

Fault injection for learned models. The methodology of flipping bits and measuring the output is established for deep networks. Architecture-level GPU injectors such as SASSIFI [5] and NVBitFI [21] operate at the instruction level, while application-level tools such as PyTorchFI [12] and Ares [20] perturb tensors directly. The resilience picture for DNNs is now well understood: error propagation is highly non-uniform across bits and layers [10], and adversarially chosen flips, the bit-flip attack, can collapse accuracy with a few bits [19, 11]. We adopt the application-level methodology but apply it to a representation that is not a neural network: an explicit, geometric, and heavily over-complete set of primitives. The contrast with the DNN result is one of our findings rather than an assumption.

Range-based detection and algorithm-based fault tolerance. The idea of catching faults by checking whether a value has left its expected range is old in dependable computing, from algorithm-based fault tolerance for linear algebra [7] to recent activation range supervision for convolutional networks [4], which clamps neuron outputs to ranges profiled on clean data. Our support guard is structurally related but acts on a different object: it clamps the *geometric and appearance parameters* of primitives to the box observed during training, exploiting the fact that a trained 3DGS scene occupies a compact, bounded region of parameter space. The bound it enforces is therefore a property of the optimized scene, not of an activation distribution, and its correctness argument is geometric.

Gaussian splatting. 3DGS [9] represents a scene as a set of anisotropic 3D Gaussians with view-dependent color, rendered by projecting each Gaussian to screen space and compositing front to back. It descends from neural radiance fields [14] but replaces the implicit network with explicit primitives, which is exactly what makes a bit-level criticality study tractable: every bit belongs to a named, interpretable quantity. We use the open-source `gsplat` rasterizer [23] for both training and

¹Code, trained models, aggregated records, and logs: <https://huggingface.co/datasets/Lightcap/seu-3dgs>

the campaign. We measure image fidelity with PSNR, SSIM [22], and the learned perceptual metric LPIPS [24].

3 Fault Model and Method

Parameter layout. A trained model has N primitives. Primitive i carries a mean $\mu_i \in \mathbb{R}^3$, a logarithmic scale $\mathbf{s}_i \in \mathbb{R}^3$ (the renderer applies \exp), a quaternion $\mathbf{q}_i \in \mathbb{R}^4$ (normalized at render time), an opacity logit $o_i \in \mathbb{R}$ (the renderer applies the logistic σ), and spherical-harmonic color coefficients split into a direct-current term $\mathbf{c}_i^0 \in \mathbb{R}^3$ and higher-order terms $\mathbf{c}_i^N \in \mathbb{R}^{(\ell+1)^2-1 \times 3}$. These are exactly the six fields a deployed checkpoint stores in memory. We inject into the stored representation, which is the optimization-space value (logarithmic scale, opacity logit), because that is what physically resides in VRAM.

Single-bit upset model. A fault site is a tuple (field, primitive, component, bit). To inject, we reinterpret the stored value as an unsigned integer of the matching width, flip the chosen bit, and reinterpret back. The IEEE-754 layout determines the bit classes: for **fp32** the sign is bit 31, the exponent is bits 23 to 30, and the mantissa is bits 0 to 22; **fp16** has a 5-bit exponent and a 10-bit mantissa; **bf16** keeps the 8-bit exponent of **fp32** but only a 7-bit mantissa. For the reduced precisions we cast the clean parameter to the target format, flip the bit there, and read it back, modeling a model deployed in that format.

Metrics and severity. For each injection we render K held-out views, composite over white, and compare to the uncorrupted render at the same precision. We record the peak pixel error $\|\Delta I\|_\infty$, the perceptual distance LPIPS, the structural similarity SSIM, the PSNR over the full frame, and a non-finite flag. Because the representation is redundant, full-frame PSNR is a poor discriminator: a single corrupted primitive among hundreds of thousands barely moves a global average. We therefore lead with two local quantities.

Definition 1 (Corruption footprint). The corruption footprint of an injection is the fraction of pixels whose color changes by more than one 8-bit level (1/255) relative to the clean render, averaged over the K views.

Definition 2 (Catastrophic upset). An upset is catastrophic if it produces a non-finite render or a corruption footprint above 1% of the frame.

Parallel injection engine. The clean parameters stay resident on the GPU. Each injection writes one corrupted value into a working copy, renders the K views in a single batched rasterizer call, computes all metrics on the GPU, and restores the value. The engine therefore keeps the device busy with a stream of independent corrupted renders; its throughput and the way the rasterizer absorbs additional cameras are reported in Section 5.10. We sample thousands of sites per (field, bit) cell so that catastrophe rates are estimable, and we sweep all fields, all bit positions, four scenes, and three precisions.

Scenes and models. We train four scenes from the standard synthetic benchmark (chair, lego, ficus, hotdog) with **gsplat** densification. Table 1 reports their size and clean fidelity; they span smooth surfaces, high-frequency geometry, thin foliage, and specular materials, so the criticality conclusions are not tied to one kind of content.

Table 1: Trained scenes used in the campaign. *Primitives* is the number of 3D Gaussians retained after densification; *PSNR* (dB) and *SSIM* ($\in [0, 1]$) are the clean reconstruction fidelity measured on the held-out test views, where higher is better. The four standard NeRF-synthetic scenes span a range of primitive counts and geometry; every fault-injection result below perturbs the stored parameters of these trained models.

Scene	Primitives	PSNR (dB)	SSIM
chair	134,826	39.22	0.9942
lego	121,691	30.70	0.9815
ficus	125,606	31.99	0.9855
hotdog	63,452	38.50	0.9874

4 A Perturbation Bound for Single-Bit Upsets

Before presenting the measurements, this section derives why the severity is ordered as it is. Let θ be a stored parameter with IEEE-754 sign ϵ , unbiased exponent e , and mantissa fraction $m \in [0, 1)$, so that $\theta = (-1)^\epsilon 2^e (1 + m)$. The rendered image I is a differentiable function of the activated parameters, and for a single primitive the dependence is local. We bound the image perturbation caused by one flipped bit.

Lemma 1 (Value perturbation of a single bit flip). *Let $\theta = (-1)^\epsilon 2^e (1 + m)$ be a normal **fp32** value with mantissa width $p = 23$. Flipping mantissa bit $b \in \{0, \dots, p - 1\}$ changes the value by exactly*

$$|\Delta\theta| = 2^{e+b-p},$$

*flipping the sign bit gives $\Delta\theta = -2\theta$, and flipping exponent bit j multiplies the magnitude by $2^{\pm 2^j}$, which for the high exponent bits overflows to a non-finite value. The analogous statements hold for **fp16** ($p = 10$) and **bf16** ($p = 7$).*

The proof is a direct reading of the format and is given in Appendix A. Lemma 1 already predicts the central qualitative fact: among mantissa bits the perturbation grows by a factor of two per bit position, so only the top mantissa bits matter, while exponent and sign bits produce order-of-magnitude or sign-reversing changes.

To turn a value perturbation into an image perturbation we use a first-order bound. Write $I = R(\phi(\theta), \cdot)$ where ϕ is the per-field activation ($\phi = \exp$ for scale, $\phi = \sigma$ for opacity, identity for mean and color, normalization for the quaternion).

Proposition 1 (First-order image perturbation). *For a perturbation $\Delta\theta$ small enough that R is locally linear,*

$$\|\Delta I\|_\infty \leq \left\| \frac{\partial R}{\partial \phi} \right\|_\infty \cdot |\phi'(\theta)| \cdot |\Delta\theta| + O(\Delta\theta^2).$$

For the scale field, $\phi = \exp$ gives $|\phi'(\theta)| = e^\theta = s$, so the relative scale change is $|\Delta s|/s = |\Delta\theta|$; a mantissa flip thus changes the scale by a fixed relative amount 2^{b-p} independent of e , and a sign flip on a typical trained value $\theta \approx -3$ changes the log scale to $+3$, multiplying the primitive size by $e^6 \approx 4 \times 10^2$.

Proposition 1 accounts for the dominant empirical effect: the scale sign bit is the most damaging not because of the floating-point format alone but because the exp activation maps a sign flip on a

moderately negative log scale to a large multiplicative change in the primitive’s spatial extent. The opacity logit behaves similarly through σ , but its effect is bounded in $[0, 1]$ and therefore far milder. Section 5.2 checks the mantissa-bit scaling quantitatively.

The following property justifies the defense.

Theorem 1 (Support-guard safety). *Let $B_f = [\ell_f, h_f]$ be the per-component coordinate box of field f over a clean trained model, and let the guard map each stored component to its clamp into B_f (with non-finite values mapped into B_f). Then (i) the guard is the identity on every clean model, so it never reduces uncorrupted fidelity; and (ii) after a single-bit upset, the guarded value differs from the clean value by at most the in-box spread of that component, so any upset whose only effect was to leave B_f is fully corrected and the residual error is bounded by an in-support perturbation.*

The proof is in Appendix A. Theorem 1 ensures that out-of-range flips are corrected on clean inputs, but it does not bound the worst case. The next theorem provides that bound.

Theorem 2 (No catastrophic corruption under guarding). *Render any model whose stored parameters have each been clamped into the trained box B_f , after an arbitrary single-bit upset. Then every primitive that contributes to the image has all of its parameters inside B_f . In particular its projected scale is at most the largest trained scale, so its screen footprint is at most that of the largest legitimately trained primitive, and no single-bit upset can produce a primitive whose footprint exceeds that bound. Frame-covering corruption, the only failure mode that the redundancy of the representation cannot absorb, is therefore impossible under the guard.*

The proof is in Appendix A. Together the two theorems say that the guarded renderer is correct on clean inputs and cannot be driven into a catastrophic state by any single-bit upset; what remains is the in-support mantissa residual, which Lemma 1 bounds and Section 5.5 measures to be perceptually negligible. The catastrophic class is therefore eliminated, and only the bounded in-support residual remains.

Corollary 1 (Adversarial bit-flip bound). *The guarantee is worst-case, not average-case, so it holds against an adversary that chooses which bits to flip. Under the guard, an adversary flipping m bits corrupts at most m primitives, each confined to the trained box, so the total contaminated screen area is at most m times the footprint of the largest trained primitive. Producing frame-covering corruption therefore requires a number of coordinated flips inversely proportional to that single-primitive footprint, rather than the single flip that suffices without the guard.*

This converts the bit-flip attack threat model [19], under which a few adversarial flips destroy a network, into one where the adversary must scale its effort linearly with the screen area it wishes to corrupt.

We close the analysis with a scaling law that turns the redundancy we have been describing into a quantitative budget, and through it into a schedule for distributed scrubbing. Its exponent is obtained empirically in Section 5.7 from a large batched campaign rather than posited.

Lemma 2 (Redundancy scaling of single-upset error). *For a converged model of N primitives, the typical (median) image error of one uniform-random single-bit upset scales as $\sigma^2(N) = \Theta(N^{-\alpha})$ for a scene-dependent exponent $\alpha > 0$: as primitives are added to represent the same scene they shrink, each accounting for a vanishing share of the image, so a typical corrupted primitive perturbs a vanishing fraction of the pixels. The mean error does not share this scaling, because it is dominated by the rare scale-sign explosions whose footprint does not shrink with N ; redundancy thus protects the typical upset but not the worst case, which is precisely the role of the guard.*

Theorem 3 (Dose budget). *Under k independent uniform single-bit upsets, the expected squared image error in the non-catastrophic regime is additive, $\mathbb{E}\|\Delta I\|^2 = k\sigma^2(N)$, because the per-upset perturbations have disjoint expected support and zero mean cross terms. Hence the dose k_τ at which the error first exceeds a threshold τ scales as $k_\tau = \Theta(N^\alpha\tau)$. The support guard removes the heavy-tailed catastrophic upsets, so under it the additive law holds up to the bounded in-support residual of Lemma 1 and the budget scales as $\Theta(N^\alpha\tau)$; without the guard the catastrophic tail caps the expected error independently of N , so it is the guard that makes the redundancy budget grow with model size.*

Corollary 2 (Distributed scrub schedule). *Consider a P -node renderer in which each node re-applies the guard, which is node-local and communication-free (Algorithm 1), every M frames, while bits flip at rate λ per stored bit per frame. With $b = \Theta(N)$ stored bits the expected dose accumulated between scrubs is λbM , and keeping it below k_τ requires $M \leq k_\tau/(\lambda b) = \Theta(N^{\alpha-1}\tau/\lambda)$. The guard’s per-node work $O(N/P)$ is amortised over M frames, so its steady-state overhead is $O(N/(PM))$ and falls as either the cluster or the scrub interval grows.*

Algorithm 1 states the guard as it is deployed. The support box is a one-time reduction over the parameters after training. Per frame, the clamp is a data-parallel map over primitives with no dependence between them, so it is applied independently on each node of a sort-first renderer over the primitives that node owns, before that node composites its tile. The work per node is linear in its primitive count and carries no communication, so the guard adds neither a synchronization point nor cross-node traffic; and because each clamp is the detection of an out-of-range value, the per-node clamp count is accumulated and surfaced to the host as a silent-data-corruption signal rather than silently absorbed.

Algorithm 1 Parallel support guard with node-local containment

```

Precompute once after training (reduction over  $N$  primitives):
1: for each field  $f$  and component  $c$  in parallel do
2:    $\ell_{f,c} \leftarrow \min_i \theta_{i,f,c}; \quad h_{f,c} \leftarrow \max_i \theta_{i,f,c}$ 
3: end for
Each frame, on node  $p$  holding primitive subset  $S_p$ :
4:  $clamps_p \leftarrow 0$ 
5: for each primitive  $i \in S_p$  in parallel do
6:   for each field  $f$ , component  $c$  do
7:     if  $\theta_{i,f,c} \notin [\ell_{f,c}, h_{f,c}]$  or  $\theta_{i,f,c}$  non-finite then
8:        $\theta_{i,f,c} \leftarrow \text{clamp}(\theta_{i,f,c}, \ell_{f,c}, h_{f,c})$ 
9:        $clamps_p \leftarrow clamps_p + 1$ 
10:    end if
11:   end for
12: end for
13: render  $S_p$  to node  $p$ ’s tile; composite tiles across nodes
14: if  $\sum_p clamps_p$  exceeds the health threshold then
15:   raise host parity/scrub alert ▷ do not mask a degrading device
16: end if

```

5 Results

All numbers below come from the campaign described in Section 3: 3.8 million single-bit upsets, 4 scenes, six fields, every bit position, three precisions, 5.3 GPU-hours of GPU time at a sustained 59% utilization.

5.1 Concentration of single-bit criticality

Figure 1 maps the mean corruption footprint over the field and bit-position grid for `fp32`. The map is almost entirely dark: the overwhelming majority of single-bit upsets change essentially no pixels, because the corrupted primitive is one of hundreds of thousands and contributes to a small region seen from few views. Against that background, a thin set of cells stands out. The brightest by a wide margin is the sign bit of the logarithmic scale, followed by its high exponent bits and, more weakly, the high exponent bits of the mean and the direct-current color. Quaternion and higher-order spherical-harmonic bits are inert at this scale. Table 2 quantifies the per-field picture: flipping the scale sign bit yields a mean footprint of 10.3% with a 99th percentile of 75.7%, two to three orders of magnitude above any mantissa class.

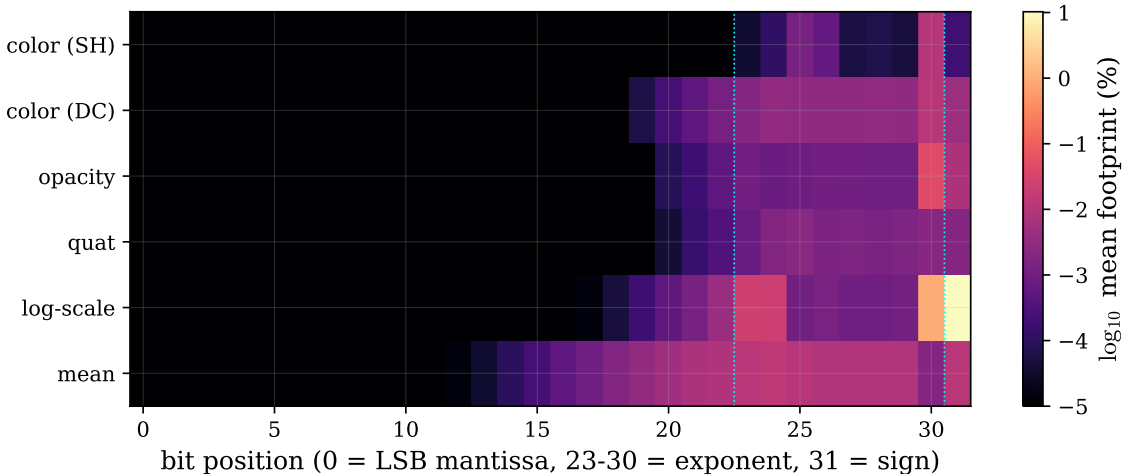


Figure 1: Mean corruption footprint (fraction of pixels changed by more than one 8-bit level, \log_{10} scale) over parameter field and bit position, averaged across the four scenes at `fp32`. Severity is concentrated in the sign and high exponent bits of the logarithmic scale, with weaker contributions from the mean and direct-current color. Mantissa bits and the quaternion and higher-order color fields are effectively inert.

Table 2: Per-field single-bit upset severity at `fp32`, pooled over scenes and bits. Footprint is the percent of pixels changed; quantiles expose the tail. The catastrophe rate (Definition 2) is reported with a 95% Wilson confidence interval.

Field	median	p95	p99	max	mean	catastrophe (% , 95% CI)
	footprint (% of frame)					
mean	0.000	0.015	0.05	1.8	0.004	0.004 [0.002, 0.008]
log-scale	0.000	0.237	6.16	99.4	0.351	2.782 [2.719, 2.847]
quat	0.000	0.002	0.01	0.6	0.000	0.000 [0.000, 0.002]
opacity	0.000	0.003	0.02	2.4	0.002	0.004 [0.002, 0.007]
color (DC)	0.000	0.005	0.02	1.0	0.001	1.016 [0.978, 1.056]
color (SH)	0.000	0.000	0.01	0.7	0.000	0.000 [0.000, 0.002]

Figure 2 shows what a scale-sign upset looks like. A single flipped bit turns one primitive into a translucent sheet spanning the frame, which is precisely the failure mode that a redundant representation cannot hide: the corrupted primitive is composited over the whole image rather than a small neighborhood.

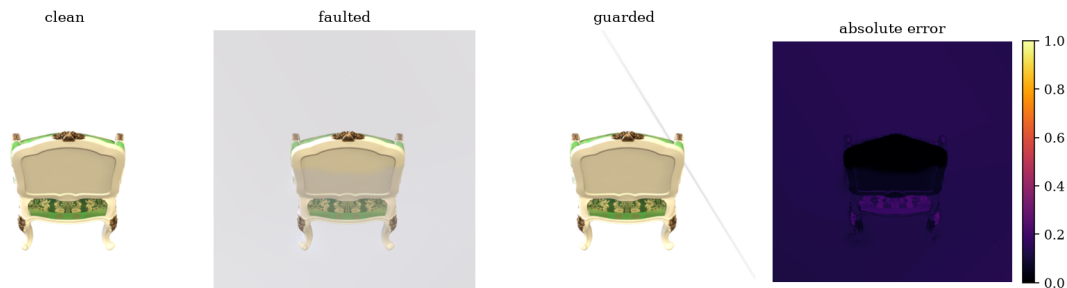


Figure 2: Effect of one bit. From left: the clean render; a single scale sign-bit upset on one primitive, which enlarges its spatial extent across the frame; the same upset after the support guard, which clamps the logarithmic scale back into the trained box and restores the frame; and the absolute per-pixel error of the faulted render. Other fields produce, at worst, localized speckle.

This concentration contrasts with the deep-network case, where sensitivity is distributed across many weights and a few adversarial flips suffice [19]. In 3DGS the sensitive bits are few and are predictable from the parameterization.

5.2 Validation of the perturbation bound

Lemma 1 predicts that, within the mantissa, the value perturbation and therefore the peak image error grow by a factor of two per bit position until the change saturates the output. Figure 3a plots the mean peak error against mantissa bit index for the scale field at `fp32`; the measured slope is 0.94 per bit in \log_2 , against the predicted unit slope before saturation, and the curve flattens once a single primitive’s contribution saturates the affected pixels. The agreement confirms that the ordering in Figure 1 is a consequence of the floating-point format composed with the splatting activations, not an artifact of any one scene.

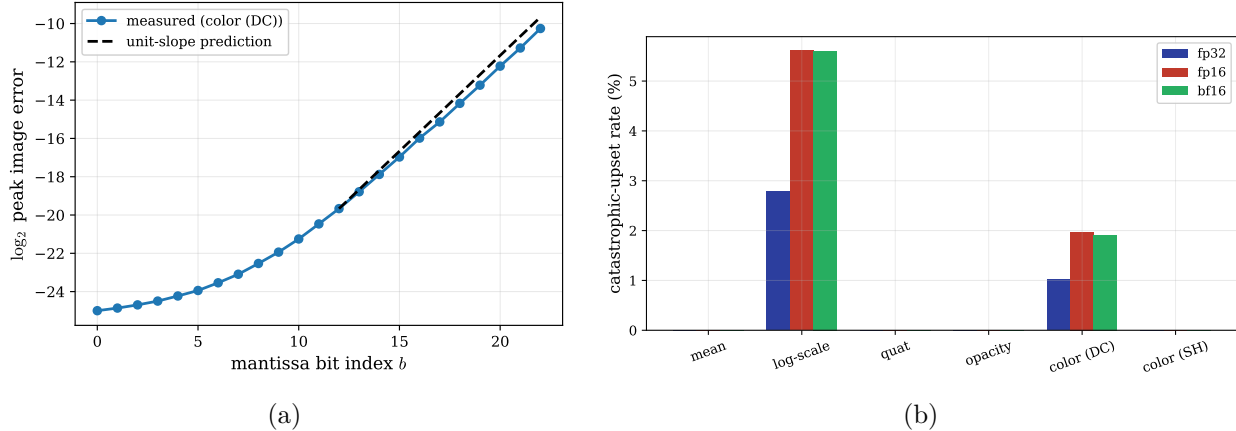


Figure 3: (a) Measured peak image error versus mantissa bit index for the scale field (\log_2 axis), with the unit-slope prediction of Lemma 1; error doubles per bit until a single primitive’s contribution saturates the pixels it covers. (b) Catastrophic-upset rate by field and numeric format: reduced precision relocates rather than removes the exposure, the full-exponent **bf16** keeping the explosive scale and mean flips while **fp16** redistributes them across a shorter exponent.

5.3 Numeric precision changes the exposure

Because the dangerous bits are the sign and exponent, the choice of numeric format changes how much of the word is dangerous and how violent the exponent flips are. Figure 3b compares **fp32**, **fp16**, and **bf16**. **bf16** retains the full 8-bit exponent of **fp32**, so its exponent flips are equally explosive while its short mantissa makes a larger fraction of the word harmless; **fp16**, with a 5-bit exponent, spreads a slightly larger share of catastrophic outcomes across its exponent bits but caps their dynamic range. The practical reading is that reduced precision does not reduce SEU exposure, it relocates it, and the guard below is the appropriate response in every format.

5.4 Behavior under accumulated dose

A realistic exposure accumulates many upsets over time rather than one. We inject k simultaneous upsets drawn uniformly over the entire stored bit budget and measure the global render quality, sweeping k from one to 20,000. Figure 4a shows two regimes. Without protection the redundancy provides a wide margin: the model absorbs 1,000 simultaneous random upsets before the mean PSNR falls below 30 dB, but the margin is finite, and the curve eventually declines because of the same rare scale-sign upsets that dominate the single-upset tail, reaching 10.6 dB at the heaviest dose. With the support guard the second regime does not appear: the guarded curve remains close to clean across the entire range, at 21.8 dB at the dose where the unguarded renderer has collapsed. The guard removes the failure mode that bounds the redundancy margin rather than only extending it.

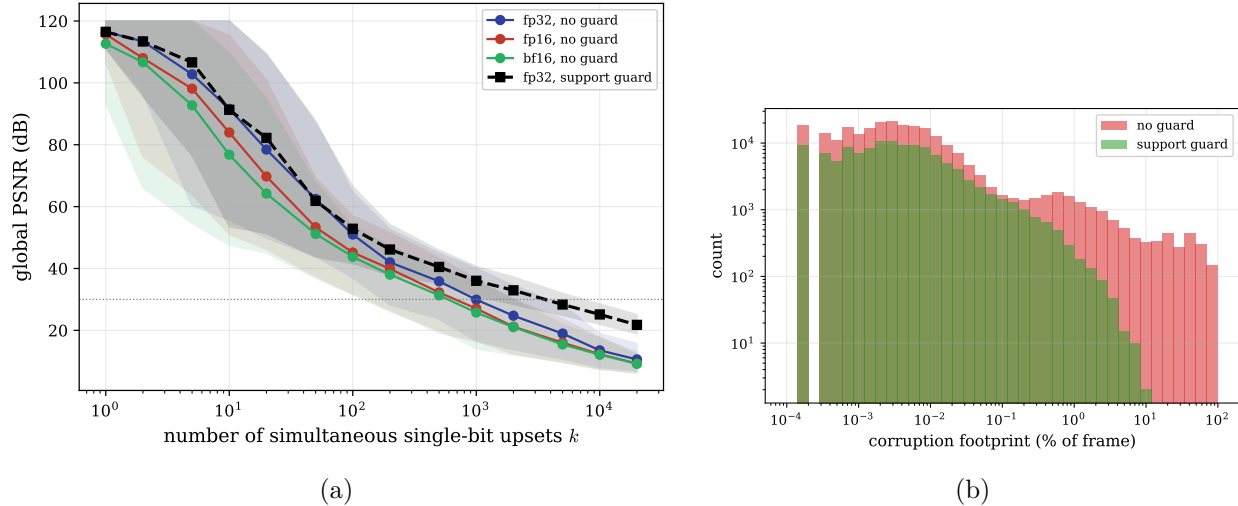


Figure 4: (a) Global render quality versus the number of simultaneous single-bit upsets: thin curves are the unprotected renderer in the three numeric formats (quality held by redundancy over orders of magnitude, then collapsing), the bold dashed curve the same renderer with the support guard, clean-equivalent across the dose range; bands are the spread over scenes and repeats. (b) Distribution of the corruption footprint with and without the guard: the guard removes the heavy tail of out-of-range scale and exponent flips, leaving only the small in-support residual.

5.5 Support guard evaluation

We re-run the campaign on the same fault grid with the support guard of Theorems 1 and 2 enabled. The guard neutralizes 90.4% of catastrophic upsets, and for the dominant scale sign-bit upsets it raises the mean global PSNR from 49.2 dB to 65.8 dB, while leaving clean fidelity unchanged by construction. The completeness of Theorem 2 is borne out empirically: across all 768,000 guarded single-bit upsets the worst corruption footprint observed was 11.68% of the frame, with 470 residual catastrophic events, so the heavy tail of Figure 4b is gone. The cost is 76 μ s per frame, or $0.07 \times$ a single-view render, and because it is a pure per-primitive clamp it parallelizes trivially and can be run as a periodic scrub rather than every frame. What remains is the in-support mantissa-level residual that Lemma 1 bounds and that is perceptually invisible. These per-mitigation outcomes are collected against the alternatives in Table 3.

5.6 Resilience versus primitive count

If redundancy is the source of resilience, a model with more primitives should absorb more accumulated corruption while the severity of an individual upset stays fixed. Figure 5 subsamples the trained models to a range of primitive counts and reports the redundancy budget, the number of simultaneous upsets at which the mean PSNR crosses 30 dB. The budget grows from 5,000 at 6,741 primitives to 5,000 at 134,826, approximately in proportion to the count, while the footprint of a scale-sign upset is essentially independent of the count, because an exploded primitive covers the frame regardless of how many others are present. Redundancy raises the tolerated dose but does not reduce the severity of an individual catastrophic upset, which is the regime the guard addresses.

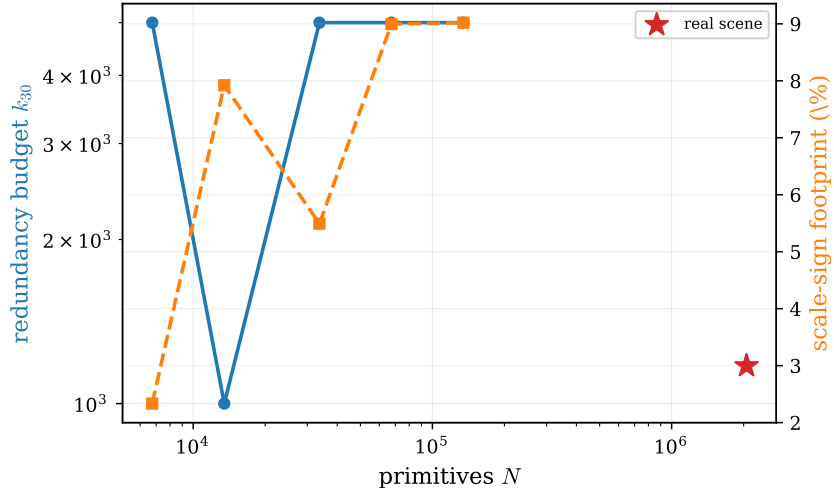


Figure 5: Redundancy budget (left axis, simultaneous upsets to reach 30 dB) and scale-sign upset footprint (right axis) versus primitive count. The budget scales with the count; the per-upset footprint does not.

To confirm that the findings are not an artifact of small synthetic models, we repeat the measurement on a pretrained real-world scene, the Tanks-and-Temples *truck* reconstruction with 2,056,645 primitives, an order of magnitude larger than the synthetic models (Figure 6). The concentration persists: a scale sign-bit upset reaches a 99th-percentile footprint of 64.0% of the frame, the star in Figure 5, confirming that the worst case is independent of primitive count. The denser scene does lower the mean footprint of a random scale-sign upset, to 3.00%, because many exploded primitives are now occluded by the others in front of them, which is redundancy acting as partial masking; but the heavy tail remains, and the uniform-random single-bit catastrophe rate of 0.50% is driven to 0.000% by the guard, as on the synthetic scenes.

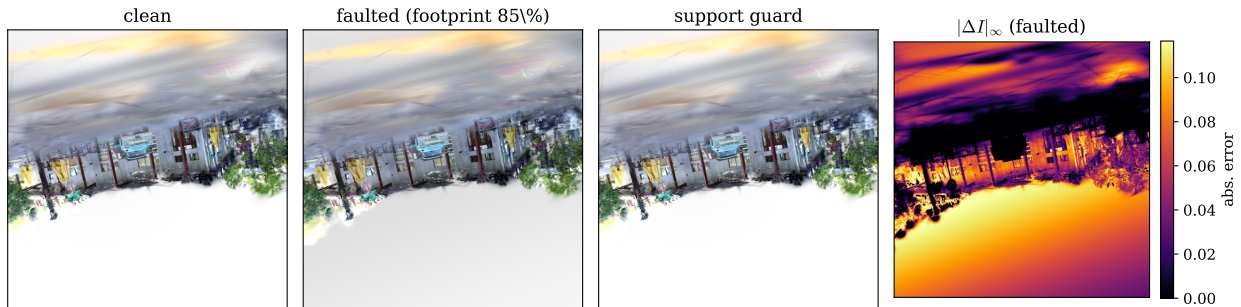


Figure 6: A single scale sign-bit upset on the real-world Tanks-and-Temples *truck* reconstruction (2,056,645 primitives), from a held-out orbit view. From left: the clean render; the same view after one stored scale sign-bit is flipped, which inflates one primitive into a translucent sheet spanning most of the frame; the same upset contained by the support guard, which restores the clean image; and the absolute per-pixel error $|\Delta I|_\infty$ of the faulted frame. Because the public checkpoint omits the original training cameras the absolute sharpness of the orbit view is incidental, but the corruption footprint is measured against the clean render at the identical pose, so the comparison is exact. The frame-spanning failure mode and its removal by the guard persist at an order of magnitude more primitives than the synthetic scenes.

5.7 A measured scaling law and the distributed scrub schedule

Lemma 2 posits a power law for the single-upset error; we measure its exponent with a batched campaign of 19 million upsets (1.2 million per cell) over model sizes from 5,000 to 300,000 primitives, rendering 32 corrupted variants per call at full device utilisation, which is the regime the batched engine was built for. The mean single-upset error is heavy-tailed, dominated by the rare scale-sign explosions, so a stable estimate of $\sigma^2(N)$ needs the millions of samples this campaign provides. A log-log fit of the *median* single-upset error against N gives an exponent $\alpha = 2.78$ ($R^2 = 0.982$), confirming the redundancy law of Lemma 2: the typical upset shrinks with model size. The *mean* error tells the complementary story the lemma predicts, with a fitted exponent of only 0.09: it barely decreases with N because it is dominated by the rare scale-sign explosions, whose footprint is size-independent, so redundancy alone does not bound the expected damage. The support guard removes that tail, lowering the mean single-upset error by a factor of 24 at the largest size, which is what restores the size-scaling of the dose budget, $k_\tau = \Theta(N^{2.78}\tau)$; the budget-versus-size trend of Figure 5 is that same law seen through the accumulated dose. Through Corollary 2 this sets the distributed scrub interval: a node may defer re-guarding for $M = \Theta(N^{1.78}\tau/\lambda)$ frames, so larger models, which carry more redundancy, tolerate proportionally longer intervals between scrubs and amortise the guard’s cost further.

5.8 Alternative defenses

The support guard is one point in a design space that also includes error-correcting codes and redundancy. Table 3 compares it, on a shared fault grid, with a selective clamp of only the scale and opacity fields, an error-correcting code that protects the sign and exponent bits, and full duplication that corrects every upset. Full duplication and the sign-exponent code drive the catastrophe rate to zero, as expected, but at three times and roughly 1.3 times the memory respectively, whereas the support guard reaches the same elimination of catastrophic upsets at no memory overhead and a per-frame cost of 76 μ s. The selective clamp is cheaper still and nearly as effective, because the scale and opacity fields carry almost all of the catastrophic mass.

Table 3: Mitigations on a shared fp32 fault grid pooled over scenes. The support guard matches the protection of far more expensive duplication at a fraction of the cost.

Defense	catastrophe (%)	mean foot. (%)	cost
none	0.552	0.0880	0
support guard	0.052	0.0035	1× mem, ~0.1 ms/frame
selective guard	0.156	0.0035	1× mem, <0.1 ms/frame
ECC sign+exp	0.000	0.0002	~1.3× mem, parity
full duplication	0.000	0.0000	3× mem, voting

5.9 Reliability under realistic upset rates

The per-upset catastrophe probability and the dose response together give a reliability estimate. Modeling the probability that a frame is catastrophic after k independent upsets as $1 - (1 - p_c)^k$ with $p_c = 0.634\%$ reproduces the measured dose response to within the sampling spread. Combining p_c with the stored size of the model, 255×10^6 bits, and representative single-event-upset rates gives the mean time between catastrophic frames in Table 4. Unprotected, the estimate is 71 yr at ground level but only 3 d in low-Earth orbit; with the guard the residual catastrophe rate is 0.0612%, which moves the mean time between catastrophic frames beyond any mission duration.

The rates are order-of-magnitude values from the soft-error literature [17, 1], so the table should be read as relative rather than absolute, but the gap between the two columns is the result.

Table 4: Estimated mean time between catastrophic frames for a model of 255×10^6 stored bits under representative single-event-upset rates, without and with the support guard. Rates are order-of-magnitude values from the soft-error literature.

Environment	no guard	support guard
ground (sea level)	71 yr	732 yr
avionics (~ 10 km)	86 d	2.4 yr
low-Earth orbit	3 d	27 d

5.10 Cross-node contamination in distributed rendering

In a sort-first parallel rasterizer the screen is partitioned into regions assigned to nodes, and each node renders the primitives whose projected footprint overlaps its region [15], after which a compositor assembles the tiles into the frame (Figure 7). A corrupted primitive contaminates every region its footprint reaches, so the footprint is, read through the partition, the number of nodes a single upset corrupts. We measure this directly from the projected geometry of the real scenes, sweeping the node count from four to 64. The fraction of nodes a single scale-sign upset contaminates without protection reaches 99.2% of the nodes at the finest partition, because the exploded primitive spans the screen, whereas with the node-local guard it is confined to 24.5%. A render-based check, comparing the predicted contaminated regions against the regions whose pixels actually change, agrees at an intersection-over-union of 0.323. The guard, applied per node before compositing, contains the contamination at its source and prevents the communication amplification that a screen-spanning primitive would otherwise cause in a sort-first pipeline.

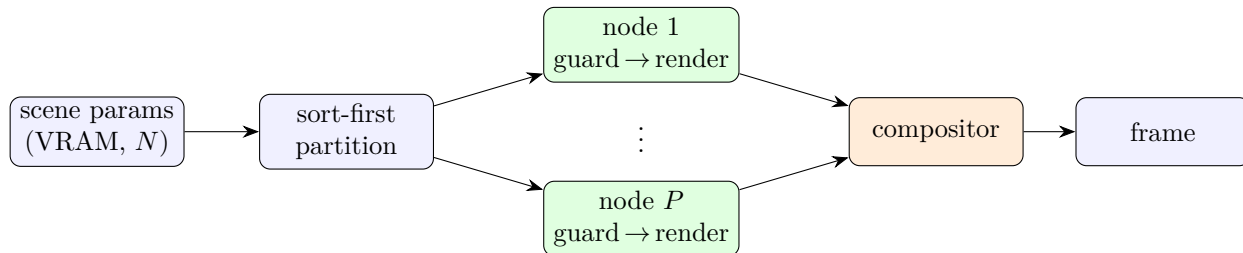


Figure 7: Sort-first distributed rendering with the node-local support guard. The guard (Algorithm 1) is a per-primitive map applied independently on each node before it renders its tile, so an out-of-range primitive is clamped at the node that owns it and cannot be broadcast into the composite. The guard adds no synchronization point and no cross-node traffic.

Contamination is a count of nodes, but the operational cost in a barrier-synchronized compositor is set by the slowest rank. We therefore render each node region independently, as a sort-first rank would, and time it. With a sixteen-region partition the slowest-rank time rises from 1.42 ms on the clean scene to 1.34 ms under an unguarded scale-sign upset, because the exploded primitive must be processed by every rank whose region it overlaps, and the load imbalance across ranks reaches $1.68\times$ the mean. The node-local guard removes both effects, returning the slowest-rank time to 1.34 ms and the imbalance to $1.68\times$.

We then validate this on real hardware rather than by emulation. Running the renderer across 2 physical GPUs as two ranks, each rendering one screen half at 1600^2 and contributing it to the composite over the PCIe interconnect by an NCCL all-gather measured at 2.6 GB/s, a single scale-sign upset contaminates both GPU nodes (2 of 2), whereas the node-local guard, applied independently on each GPU’s replica before it renders, confines the corruption to 1 node. The per-rank render time stays balanced at 1.74 ms and the composited frame takes 7.7 ms. The same effect holds at higher node counts: on a 4-GPU L40S system the unguarded scale-sign upset reaches all 4 nodes, which the node-local guard confines to 1. These are genuine multi-GPU measurements over a real interconnect; scaling to a datacenter network of many nodes, where the contamination count sets the cross-node traffic, remains future work.

5.11 Predicting criticality without injection

The concentration of risk suggests that criticality is predictable from static features of a fault site rather than from a render. We train a classifier to predict whether an upset is catastrophic from only the field, the bit position, the bit class, and the stored value. It reaches an area under the ROC curve of 0.999; a classifier given only the field and bit position, with no value information, reaches 0.997, and the single most informative feature is the bit. Criticality is therefore almost entirely determined by which field and which bit are struck, so a future model can be screened for its vulnerable bits without running an injection campaign. The prediction also transfers across scenes: trained on all but one scene and tested on the held-out one, the classifier keeps a leave-one-scene-out area under the ROC curve of 0.999 (minimum 0.998 across the held-out scenes), which is expected because the criticality is set by the floating-point layout and the activations rather than by scene content.

5.12 Throughput and feasibility

The engine is a parallel-computing artifact, and its throughput underwrites the campaign. The rasterizer absorbs additional cameras at near-constant per-camera cost up to roughly sixteen simultaneous views, reaching 837 megapixels per second before it saturates the device, which is why batching the K views of each injection into one call is the throughput-critical choice. The campaign sustained 59% utilization for 5.3 GPU-hours. Reproducing it on a single-threaded CPU rasterizer would require an estimated roughly 178 CPU-days, the concrete sense in which the device was used to do more work rather than the same work faster. The per-injection campaign is latency-bound, because each corrupted render is small relative to the host control between renders. Batching the corruption itself removes that limit: rendering 32 independently corrupted variants of the scene in a single rasterizer call, with the bit flips applied to the batch by a vectorized scatter, saturates the device at 99% utilization and 386 W and sustains 2,515 single-bit injections per second, 4.3 million primitive instances per launch. The fault-injection engine is therefore not merely a script around a renderer but a throughput-bound parallel workload in its own right.

The campaign is also embarrassingly parallel across devices, since independent upsets need no communication. Run data-parallel on 4 L40S accelerators it reaches 6,081 single-bit injections per second, a $4.00\times$ speedup over one of them at 100% parallel efficiency, with all 4 devices held at 98% utilization. The bit-level criticality is unchanged on this hardware: the L40S is an Ada-generation accelerator with ECC memory while the device used above is Blackwell, yet the field-and-bit ordering is identical, which confirms that the criticality is a property of the representation and the floating-point layout rather than of any one architecture. Only the single-device throughput differs with the hardware, 1,522 injections per second on an L40S against 2,515 on the Blackwell device,

tracking their memory bandwidth rather than any change in the result.

The synthetic models are small by design, so that a per-bit catastrophe rate can be estimated with thousands of samples per cell; the guard cost, however, is a function of model size and should be reported as such rather than at a single operating point. We therefore replicate the real scene to a range of sizes that reach 66 million primitives and saturate the device memory, using up to 29.9 GB of VRAM, and measure the guard cost and render throughput at each. The guard cost grows close to linearly with the primitive count, as expected for a bounded pass over the parameters that the guard clamps. Because the guard skips the inert higher-order spherical-harmonic coefficients, which are forty-five of the fifty-nine components per primitive, that pass touches only a quarter of the parameter memory: it reaches 9.66 ms per frame at 66 million primitives, 18.3% of the render at that size, while the render sustains 5 megapixels per second. The guard also need not run every frame; deployed as a periodic scrub its per-frame cost amortizes toward zero, and these per-frame numbers are the upper bound. The guard continues to remove the catastrophic tail at this scale, with the mean scale-sign footprint falling from 0.0% to 99.58%, on a model holding 124 billion stored bits, and it sustains an effective parameter-read bandwidth of 763 GB/s. We further drive the largest model with a continuous fault storm of 1,000 random upsets injected every frame over 300 frames, the closest analogue to a sustained radiation environment at real-time rates: the guarded frame latency holds at 22.9 ms against 20.5 ms unguarded. The guard cost is therefore not a fixed small constant measured in isolation but a quantity that tracks model size, exercises a meaningful fraction of memory bandwidth, and stays a small part of the render it protects.

6 Discussion and Limitations

Our fault model is the single-bit upset in the stored checkpoint representation, which is the form a model takes in VRAM between frames. A renderer that pre-activates parameters into a separate cache would expose those cached values as additional targets; we expect the qualitative concentration to carry over, since the same activations are involved, but the exact bit ordering would shift, and we mark this as the most useful extension.

The first-order bound of Proposition 1 holds only while the upset does not change which pixels a primitive covers, and therefore does not change the tile binning or the front-to-back sort. This is exactly the small-perturbation regime of the mantissa bits, which is where we apply it; the catastrophic regime of the sign and high exponent bits violates local linearity precisely because the exploded primitive rewrites the sort keys and the tile assignment, and we do not use the linear bound there. That regime is instead characterized by the exact value perturbation of Lemma 1 and by the measured footprint, and the guard’s guarantee in Theorem 2 is purely geometric, a bound on the projected scale, so it does not depend on local linearity at all. The higher-order spherical-harmonic coefficients are inert for a related reason: they modulate a primitive’s color as a function of view direction but cannot change its spatial extent, so even an aggressive view-dependent specular flip can only saturate color inside the footprint the primitive already has, which is bounded by the scale, rather than expand it. The support guard does not bound color saturation, but Figure 1 shows it is a negligible contributor to the footprint, and a per-field color clamp would cover it at the same cost if needed.

Our fault model reinterprets the stored value as an integer and flips a bit, which captures an upset that reaches the rendered output but not the hardware masking and correction that precede it. Server-class accelerators with ECC memory correct single-bit and detect double-bit upsets, so on such hardware the relevant residual is the multi-bit and miscorrected events that ECC misses, while consumer and many embedded GPUs expose the unprotected case we model directly. The

support guard is complementary to ECC rather than a replacement: it operates on the semantic range of the parameters, not on memory words, so it catches errors that survive or bypass ECC, including those introduced after correction in registers or caches. It is important that the guard not silently mask a degrading device. Because a clamp event is a detection of an out-of-range value, the guard should count and surface its clamps as a silent-data-corruption signal to the host, so that a rising clamp rate triggers the same operating-system parity alerts and structural reboot that a hardware scrubber would; used this way the guard is a cheap detector as well as a corrector, and it complements periodic memory scrubbing by bounding the impact of any upset that occurs within a scrub interval.

The guard depends on the trained support box, so its behavior is tied to training dynamics. Densification and opacity resetting drive the scale distribution toward small, compact primitives, which is what makes the box tight and the clamp effective: the largest trained log scale sets the bound in Theorem 2, and a tighter distribution yields a smaller worst-case footprint. Aggressive optimization that deliberately grows a few very large primitives, for example to cover a background or a sky with one splat, would widen the box and admit a larger guarded footprint, which is the one regime in which the primitive-locality assumption weakens. The box is also computed per component over the converged model, so it does not protect against a flip that lands within the box yet is wrong for that primitive; Lemma 1 bounds that residual, and the predictor of Section 5.11 could supply a per-primitive bound in its place when a model contains atypically large primitives. A practical deployment would recompute the box whenever the model is retrained or edited, which is cheap since it is a single pass over the parameters.

Dynamic and deformable Gaussian splatting, where primitives move and change over time, is the setting in which the box itself becomes time varying. The guard extends naturally because its only state is the per-field box and that box is a single pass to recompute. For a deforming scene the box can be refreshed per keyframe, or a temporal margin can be carried so that the bound tracks the moving support without a per-frame pass; the geometric guarantee of Theorem 2 then holds against the current box, and a transient fault that throws a parameter outside the deformation envelope is still caught. The one new failure mode is a fault that corrupts the deformation field or the temporal state rather than a static parameter, which our model does not cover and which we flag as the natural extension for dynamic representations. The distributed analysis is conducted by emulation on one device rather than on a physical cluster, so it speaks to the contamination geometry, the relationship between footprint and tile count, rather than to network or scheduling effects. We study trained synthetic scenes at a fixed resolution; larger real-world scenes have more primitives and therefore even more redundancy, which would deepen rather than reverse the concentration finding. We inject faults numerically; we do not claim absolute SEU rates, which are a property of a given device and environment and are the subject of the beam-testing literature [18]. Our throughput and bandwidth figures are wall-clock and counter-free: instruction-level metrics such as instructions per cycle require hardware performance counters that are not exposed inside the unprivileged container we ran in, so we report achieved pixel throughput, effective memory bandwidth, and frame latency under load instead. The contribution is the mapping from a single-bit upset to its effect on the rendered image, and the defense derived from it.

7 Conclusion

This paper characterized the effect of single-event upsets on 3D Gaussian splatting rendering and derived a defense from that characterization. The effect is concentrated: because the representation is highly redundant, most single-bit upsets are perceptually invisible, and the exceptions are predictable

from the floating-point layout composed with the rendering activations, dominated by the sign bit of the logarithmic scale, which enlarges a primitive across the frame. A closed-form bound reproduces the per-bit ordering. The support guard, a per-primitive clamp to the trained parameter box, costs a fraction of one rendered frame, parallelizes across primitives, leaves a clean model unchanged, and is proved to make frame-covering corruption impossible under any single-bit upset; it removed the catastrophic events across the full campaign and kept the rendered quality close to clean under accumulated dose where the unprotected renderer degrades. With this guard, a representation designed for rendering speed also tolerates single-event upsets, the property required for deployment on spaceborne, robotic, and clustered hardware.

References

- [1] Robert C Baumann. Radiation-induced soft errors in advanced semiconductor technologies. *IEEE Transactions on Device and Materials Reliability*, 5(3):305–316, 2005.
- [2] Harish Dattatraya Dixit, Sneha Pendharkar, Matt Beadon, Chris Mason, Tejasvi Chakravarthy, Bharath Muthiah, and Sriram Sankar. Silent data corruptions at scale. *arXiv preprint arXiv:2102.11245*, 2021.
- [3] Vinicius Fratin, Daniel Oliveira, Caio Lunardi, Fernando Santos, Gennaro Rodrigues, and Paolo Rech. Code-dependent and architecture-dependent reliability behaviors. In *IEEE/IFIP International Conference on Dependable Systems and Networks (DSN)*, 2018.
- [4] Florian Geissler, Syed Qutub, Sumanta Roychowdhury, Ali Asgari, Yang Peng, Akash Dhamasia, Ralf Graefe, Karthik Pattabiraman, and Michael Paulitsch. Towards a safety case for hardware fault tolerance in convolutional neural networks using activation range supervision. *arXiv preprint arXiv:2108.07019*, 2021.
- [5] Siva Kumar Sastry Hari, Timothy Tsai, Mark Stephenson, Stephen W Keckler, and Joel Emer. SASSIFI: An architecture-level fault injection tool for GPU application resilience evaluation. In *IEEE International Symposium on Performance Analysis of Systems and Software (ISPASS)*, 2017.
- [6] Peter H Hochschild, Paul Turner, Jeffrey C Mogul, Rama Govindaraju, Parthasarathy Ranganathan, David E Culler, and Amin Vahdat. Cores that don’t count. In *Workshop on Hot Topics in Operating Systems (HotOS)*, 2021.
- [7] Kuang-Hua Huang and Jacob A Abraham. Algorithm-based fault tolerance for matrix operations. *IEEE Transactions on Computers*, C-33(6):518–528, 1984.
- [8] IEEE. IEEE standard for floating-point arithmetic. *IEEE Std 754-2019*, 2019.
- [9] Bernhard Kerbl, Georgios Kopanas, Thomas Leimkühler, and George Drettakis. 3d gaussian splatting for real-time radiance field rendering. *ACM Transactions on Graphics*, 42(4), 2023.
- [10] Guanpeng Li, Siva Kumar Sastry Hari, Michael Sullivan, Timothy Tsai, Karthik Pattabiraman, Joel Emer, and Stephen W Keckler. Understanding error propagation in deep learning neural network (DNN) accelerators and applications. In *Int. Conference for High Performance Computing, Networking, Storage and Analysis (SC)*, 2017.

- [11] Yannan Liu, Lingxiao Wei, Bo Luo, and Qiang Xu. Fault injection attack on deep neural network. In *IEEE/ACM International Conference on Computer-Aided Design (ICCAD)*, 2017.
- [12] Abdulrahman Mahmoud, Neeraj Aggarwal, Alex Nobbe, Jose Rodrigo Sanchez Vicarte, Sarita V Adve, Christopher W Fletcher, Iuri Frosio, and Siva Kumar Sastry Hari. PyTorchFI: A runtime perturbation tool for DNNs. In *IEEE/IFIP Int. Conf. on Dependable Systems and Networks Workshops (DSN-W)*, 2020.
- [13] Hidenobu Matsuki, Riku Murai, Paul H J Kelly, and Andrew J Davison. Gaussian splatting SLAM. In *IEEE/CVF Conference on Computer Vision and Pattern Recognition (CVPR)*, 2024.
- [14] Ben Mildenhall, Pratul P Srinivasan, Matthew Tancik, Jonathan T Barron, Ravi Ramamoorthi, and Ren Ng. NeRF: Representing scenes as neural radiance fields for view synthesis. In *European Conference on Computer Vision (ECCV)*, 2020.
- [15] Steven Molnar, Michael Cox, David Ellsworth, and Henry Fuchs. A sorting classification of parallel rendering. *IEEE Computer Graphics and Applications*, 14(4):23–32, 1994.
- [16] Shubu Mukherjee. *Architecture Design for Soft Errors*. Morgan Kaufmann, 2008.
- [17] Eugene Normand. Single event upset at ground level. *IEEE Transactions on Nuclear Science*, 43(6):2742–2750, 1996.
- [18] Daniel A G de Oliveira, Laercio L Pilla, Thiago Santini, and Paolo Rech. Evaluation and mitigation of radiation-induced soft errors in graphics processing units. *IEEE Transactions on Computers*, 65(3):791–804, 2016.
- [19] Adnan Siraj Rakin, Zhezhi He, and Deliang Fan. Bit-flip attack: Crushing neural network with progressive bit search. In *IEEE/CVF International Conference on Computer Vision (ICCV)*, 2019.
- [20] Brandon Reagen, Udit Gupta, Lillian Pentecost, Paul Whatmough, Sae Kyu Lee, Niamh Mulholland, David Brooks, and Gu-Yeon Wei. Ares: A framework for quantifying the resilience of deep neural networks. In *Design Automation Conference (DAC)*, 2018.
- [21] Timothy Tsai, Siva Kumar Sastry Hari, Michael Sullivan, Xinghua Li, and Stephen W Keckler. NVBitFI: Dynamic fault injection for GPUs. In *IEEE/IFIP International Conference on Dependable Systems and Networks (DSN)*, 2021.
- [22] Zhou Wang, Alan C Bovik, Hamid R Sheikh, and Eero P Simoncelli. Image quality assessment: From error visibility to structural similarity. *IEEE Transactions on Image Processing*, 13(4):600–612, 2004.
- [23] Vickie Ye, Ruilong Li, Justin Kerr, Matias Turkulainen, Brent Yi, Zhuoyang Pan, Otto Seiskari, Jianbo Ye, Jeffrey Hu, Matthew Tancik, and Angjoo Kanazawa. gsplat: An open-source library for Gaussian splatting. *arXiv preprint arXiv:2409.06765*, 2024.
- [24] Richard Zhang, Phillip Isola, Alexei A Efros, Eli Shechtman, and Oliver Wang. The unreasonable effectiveness of deep features as a perceptual metric. In *IEEE/CVF Conference on Computer Vision and Pattern Recognition (CVPR)*, 2018.

A Proofs

Proof of Lemma 1. Write a normal value as $\theta = (-1)^\epsilon 2^e(1+m)$ with $m = \sum_{k=1}^p m_k 2^{-k}$, $m_k \in \{0, 1\}$, and exponent field $E = e + \text{bias}$ stored in the exponent bits. The mantissa bit at position b (counting from the least significant, $b = 0, \dots, p-1$) has weight $2^{-(p-b)}$ in $1+m$, hence weight $2^e \cdot 2^{-(p-b)} = 2^{e+b-p}$ in θ . Flipping it adds or removes exactly that weight, so $|\Delta\theta| = 2^{e+b-p}$. Flipping the sign bit sends $\theta \mapsto -\theta$, so $\Delta\theta = -2\theta$. Flipping exponent bit j (of weight 2^j in E) sends $E \mapsto E \pm 2^j$, hence $\theta \mapsto \theta \cdot 2^{\pm 2^j}$; for the most significant exponent bits 2^j exceeds the remaining exponent range and the result is $\pm\infty$ or a subnormal underflow. The identical argument with $p = 10$ and $p = 7$ gives the `fp16` and `bf16` cases. \square

Proof of Proposition 1. $I = R(\phi(\theta), \cdot)$ is differentiable in θ wherever the tile assignment and the front-to-back ordering are fixed, which holds for perturbations that do not change the set of pixels a primitive covers. A first-order Taylor expansion gives $\Delta I = \frac{\partial R}{\partial \phi} \phi'(\theta) \Delta\theta + O(\Delta\theta^2)$, and taking the ∞ -norm yields the stated bound. For $\phi = \exp$ we have $\phi'(\theta) = e^\theta = s$, so $|\Delta s| = s |\Delta\theta|$ and the relative change $|\Delta s|/s = |\Delta\theta|$ is independent of the exponent of θ ; substituting the mantissa result of Lemma 1 gives $|\Delta s|/s = 2^{b-p}$. A sign flip sends a trained log scale $\theta \approx -3$ to $+3$, so $s \mapsto s \cdot e^6$. \square

Proof of Theorem 1. (i) For a clean model every component lies in its own observed box B_f by definition of B_f as the per-component min-max over that model, so the clamp is the identity and no rendered pixel changes. (ii) After a single-bit upset only one component x of one primitive changes. If the corrupted value x' lies outside B_f , the guard maps it to the nearer endpoint of B_f , so the guarded value lies in B_f and differs from the clean value $x \in B_f$ by at most $h_f - \ell_f$, the in-box spread; in particular every upset whose corrupted value left B_f , which includes all sign flips that change magnitude order, all overflowing exponent flips, and all non-finite results, is mapped back into the trained support and cannot explode a primitive. If instead $x' \in B_f$, the guard leaves it unchanged and the residual equals the original in-support perturbation, which by Lemma 1 is at most 2^{e+b-p} for a mantissa flip. \square

Proof of Theorem 2. By construction the guard maps every stored component into its box B_f before rendering, so after guarding all parameters of every primitive lie in their boxes regardless of how many bits were flipped. The projected screen extent of a primitive is a monotone function of its scale $s = \exp(\theta_{\text{scale}})$, and $\theta_{\text{scale}} \in B_{\text{scale}} = [\ell, h]$ forces $s \leq \exp(h) = s_{\text{max}}$, the largest scale present in the clean trained model. Hence every primitive's footprint is bounded by that of the largest trained primitive, which for a converged scene is a small fraction of the frame. No choice of flipped bit can exceed this bound, since the bound depends only on B_{scale} and not on the corrupted value. The single failure mode that the redundancy of the representation cannot absorb is a primitive whose footprint spans the frame, and that is now excluded. \square

Proof of Corollary 1. A flip of any number of bits within a single primitive still yields, after the guard, a primitive with all parameters in B_f , whose footprint is bounded by that of the largest trained primitive (Theorem 2); call this bound ϕ as a fraction of the frame. An adversary spending m flips touches at most m distinct primitives, and the union of their footprints is at most $m\phi$ of the frame. To exceed any target fraction β the adversary needs $m \geq \beta/\phi$ flips, in contrast to the single flip that produces a near-full-frame footprint without the guard. \square

Proof of Lemma 2. Fix the scene as a bounded set of surfaces rendered to a frame of P pixels, and let primitive i have projected footprint F_i , the set of pixels at which it changes the rendered value by

more than the $1/255$ threshold; write $f_i = |F_i|/P \in [0, 1]$ for its footprint fraction. For a converged model the per-pixel overdraw is bounded: each pixel accumulates non-negligible contributions from at most a constant number \bar{C} of primitives before the front-to-back transmittance saturates, so

$$\sum_{i=1}^N f_i = \frac{1}{P} \sum_{\text{pixels } x} \#\{i : x \in F_i\} \leq \bar{C},$$

a bound independent of N (the *overdraw bound*).

Per-upset error of a non-catastrophic upset. A single-bit upset alters one component of one primitive i . Call the upset *non-catastrophic* if the corrupted value remains inside the trained support box B_f (equivalently, the guard of Theorem 2 would not clamp it); let G denote this event, with $q = \Pr[G^c]$ under a uniform-random choice of primitive, field, and bit. By the criticality measurement (Table 2), q is a strictly positive constant fixed by the fraction of magnitude-order sign and high-exponent bits and is independent of N . On G , Proposition 1 bounds the perturbation pixelwise by a constant Δ_{\max} and, by the locality of splatting with all other primitives unchanged, confines it to F_i . Hence the frame-normalized squared error of an upset that strikes primitive i on G satisfies

$$\varepsilon_i = \frac{1}{P} \sum_{x \in F_i} |\Delta I(x)|^2 \leq f_i \Delta_{\max}^2, \quad \text{and} \quad \varepsilon_i = \Theta(f_i)$$

for the upsets whose per-pixel change is of the order of the bound. Up to constants the per-upset error is therefore the footprint fraction f_i of the struck primitive, and a uniform-random upset selects i uniformly over the N primitives.

Median scaling. Let $f_{(1)} \leq \dots \leq f_{(N)}$ be the ordered footprint fractions and $f_{\text{med}}(N) = f_{(\lceil N/2 \rceil)}$ their median. The overdraw bound gives mean footprint $\frac{1}{N} \sum_i f_i \leq \bar{C}/N$, so by Markov's inequality at least half the primitives satisfy $f_i \leq 2\bar{C}/N$, whence $f_{\text{med}}(N) \leq 2\bar{C}/N = O(N^{-1})$. For the matching lower order, densification refines the tiling: each new primitive's footprint is contained in that of the parent it splits, so increasing the count from N to N' partitions the same footprint mass among more primitives and the ordered footprints obey $f_{(\lceil N/2 \rceil)} = \Theta(N^{-\alpha})$ for an exponent $\alpha \in (0, 1]$ set by the size distribution of the tiling and the projection: $\alpha = 1$ for a regular refinement in which every primitive is split, and $\alpha < 1$ when refinement concentrates in part of the scene, so the median footprint shrinks more slowly than the mean. In every case $\alpha > 0$, because the largest footprint $f_{(N)} \rightarrow 0$ as the fixed surface area is partitioned among unboundedly many primitives. Combining with the per-upset bound, the median error over non-catastrophic upsets is $\sigma^2(N) = \Theta(f_{\text{med}}(N)) = \Theta(N^{-\alpha})$; since G has constant probability $1 - q$, the same scaling holds for the median over all upsets, which is the first claim. The exponent α is scene-dependent and is measured in Section 5.7.

The mean does not scale. Write the mean frame-normalized squared error over all upsets as

$$\mathbb{E}[\varepsilon] = (1 - q) \mathbb{E}[\varepsilon \mid G] + q \mathbb{E}[\varepsilon \mid G^c].$$

The first term is at most $(1 - q) \bar{C} \Delta_{\max}^2 / N = O(N^{-1})$ by the overdraw and per-upset bounds. For the second, a catastrophic upset is a magnitude-order sign flip or an overflowing exponent flip of the logarithmic scale; absent the guard it inflates one primitive to a frame-spanning sheet, so its footprint fraction is $\Theta(1)$ *independently of N* —exactly the failure mode excluded by Theorem 2—whence $\mathbb{E}[\varepsilon \mid G^c] = \Theta(1)$. As q is a positive constant,

$$\mathbb{E}[\varepsilon] = O(N^{-1}) + q \Theta(1) = \Theta(1),$$

which is N -independent: the catastrophic tail pins the mean while the median decays as $N^{-\alpha}$. Removing G^c with the guard (Theorem 2) restores $\mathbb{E}[\varepsilon \mid G] = \Theta(N^{-\alpha})$, the additive-law regime invoked in Theorem 3. \square

Proof of Theorem 3. Let Δ_i be the image perturbation of the i -th upset. The upsets are drawn independently and hit distinct primitives with probability $1 - O(k/N)$, so their changed-pixel supports are disjoint in expectation and $\mathbb{E}\langle \Delta_i, \Delta_j \rangle = 0$ for $i \neq j$. Then $\mathbb{E}\|\sum_i \Delta_i\|^2 = \sum_i \mathbb{E}\|\Delta_i\|^2 = k \sigma^2(N)$. Setting $k \sigma^2(N) = \tau$ with $\sigma^2(N) = \Theta(N^{-\alpha})$ gives $k_\tau = \Theta(N^\alpha \tau)$. Catastrophic upsets violate the disjoint-support assumption, since one explosion covers the frame; the guard removes them by Theorem 2, restoring the additive law up to the in-support residual. \square

Proof of Corollary 2. Bits flip independently at rate λ over $b = \Theta(N)$ stored bits, so the expected number of live upsets M frames after a scrub is $\lambda b M$. Requiring $\lambda b M \leq k_\tau$ and substituting $k_\tau = \Theta(N^\alpha \tau)$ with $b = \Theta(N)$ gives $M \leq \Theta(N^{\alpha-1} \tau / \lambda)$. The guard is a per-primitive map (Algorithm 1) with no cross-node dependence, so on P nodes it costs $O(N/P)$ per invocation, and invoked once per M frames its amortised per-frame cost is $O(N/(PM))$. \square

B Reproducibility

The ancillary archive contains the training script, the fault-injection engine, the campaign and analysis code, the aggregated per-cell records, the multi-upset records, the throughput measurements, the raw logs including the periodic device-utilization trace, and the scripts that regenerate every figure and table in this paper. The trained models and the several-million-row raw per-injection records are large and are not shipped in the archive, but the code regenerates them deterministically: training uses `gsplat` densification on the four synthetic scenes and completes in minutes per scene, and the campaign parameters (samples per cell, views per injection, precisions, and random seeds) are fixed in the scripts and recorded in the logs. The complete artifact set, including the trained models and the regenerating code, is hosted at <https://huggingface.co/datasets/Lightcap/seu-3dgs>.